# Iterative Detection-Decoding of Interleaved Hermitian Codes for High Density Storage Devices

Li Chen, *Senior Member, IEEE*, Martin Johnston, and Gui Yun Tian, *Senior Member, IEEE*

***Abstract*—Traditionally, Reed-Solomon (RS) codes have been employed in magnetic data storage devices due to their effectiveness in correcting random errors and burst errors caused by thermal asperities and inter-symbol interference (ISI). However, as storage densities increase the effect of ISI becomes more severe and much longer RS codes are needed, but this requires significantly increasing the size of the finite field. A possible replacement for RS codes are the one-point Hermitian codes, which are a class of algebraic-geometric (AG) code that have larger block sizes and minimum Hamming distances over the same finite field. In this paper, we present a novel iterative soft detection-decoding algorithm for interleaved Hermitian codes. The soft decoding employs a joint adaptive belief propagation (ABP) algorithm and Koetter-Vardy (KV) list decoding algorithm. It is combined with a maximum *a posteriori* (MAP) partial response (PR) equalizer and likelihoods from the output of the KV or the ABP algorithm are fed back to the equalizer. The proposed scheme's iterative detection-decoding behavior will be analyzed by utilizing the Extrinsic Information Transfer (ExIT) chart. Our simulation results demonstrate the performance gains achieved by iterations and Hermitian codes' performance advantage over RS codes.**

***Index Terms*—Belief propagation (BP), Hermitian codes, iterative methods, Koetter-Vardy algorithm, partial response channel.**

## I. Introduction

ALGEBRAIC-GEOMETRIC (AG) codes were presented by Goppa in 1981 [1] and are a class of non-binary block codes constructed from the points on some affine curves. It is desirable to maximize the number of points as this results in AG codes with very long codewords and large minimum Hamming distances. For this reason, Hermitian curves are a popular choice of curve for constructing AG codes as one can achieve the maximal ratio between the number of affine points and its genus. Conventional Reed-Solomon (RS) codes can be viewed as the simplest type of AG code, constructed from the points on an affine line. However, the length of RS codewords is limited by the size of the finite field it is defined in since generally there are fewer points on an affine line than an affine curve. Johnston *et al.* [2] evaluated the performance of Hermitian codes using Sakata's algorithm [3] and showed that significant coding gains could be achieved over RS codes defined in the same finite field. Further improvements in performance can be achieved with list decoding by using the Guruswami-Sudan (GS) algorithm [4], which can correct errors beyond the half distance bound. Hoholdt *et al.* [5] presented a list decoding algorithm for Hermitian codes by defining the interpolation property of a trivariate polynomial that is defined over the pole basis of a Hermitian curve. Chen *et al.* [6] were the first to evaluate the list decoding performance of Hermitian codes and at the same time presented a method to reduce the decoding complexity. GS algorithm was later modified by Koetter and Vardy [7] to obtain a soft-decision list decoding algorithm for RS codes, known as the Koetter-Vardy (KV) algorithm. Chen *et al.* [8] and Lee *et al.* [9] then independently developed a KV algorithm for Hermitian codes outperforming GS algorithm. Recently, Chen showed how the iterative decoding of Hermitian codes could be achieved by proposing the serial concatenation of an inner adaptive belief propagation (ABP) algorithm and an outer KV algorithm [10]. The ABP algorithm operates on an adapted binary parity-check matrix of a Hermitian code and enhances the reliability of the soft received information [11].

Due to a Hermitian code's very large minimum Hamming distance, it is ideally suited to channels that exhibit many burst errors and random errors, such as magnetic storage channels. Interleaved Hermitian codes comprise a number of Hermitian codewords interleaved using a block interleaver, allowing the codewords to assist each other during the decoding process. The codeword length is also effectively increased without increasing the size of finite field. In this paper, a turbo-like iterative detection-decoding scheme that integrates maximum *a posteriori* (MAP) [12] channel equalization and iterative soft decoding [10] of interleaved Hermitian codes is designed for partial response (PR) channels. The application of turbo equalization to magnetic storage channels is a well-known technique for the joint detection and decoding of read data and is commonly performed using the low-density parity-check (LDPC) codes [13], [14]. Although LDPC codes perform well with turbo equalization on magnetic channels, they are susceptible to error floors at low bit-error rates (BER) and since they

Manuscript received December 22, 2013; revised May 23, 2014 and August 10, 2014; accepted August 13, 2014. Date of publication September 11, 2014; date of current version October 17, 2014. This work was supported by the National Natural Science Foundation of China (NSFC) under Grant 61372079, the National Basic Research Program of China (973 Program) under Grant 2012CB316100 and the EU 7th Framework Programme project Health Monitoring of Offshore Wind Farms (HEMOW) (FP7/2007-2013) for funding the CONHEALTH project under Grant FP7-PEOPLE-2011-IRSES No. 294923. The associate editor coordinating the review of this paper and approving it for publication was K. Abdel-Ghaffar.

L. Chen is with the School of Information Science and Technology, Sun Yat-sen University, Guangzhou 510275, China (e-mail: chenli55@mail.sysu.edu.cn; sist.sysu.edu.cn/~chenli).

M. Johnston and G. Y. Tian are with the School of Electrical and Electronic Engineering, Newcastle University, Newcastle NE1 7RU, U.K. (e-mail: martin.johnston@ncl.ac.uk; g.y.tian@ncl.ac.uk).

Digital Object Identifier 10.1109/TCOMM.2014.2357026

are binary they are not as effective at correcting burst errors. Our proposed iterative decoding algorithm has been designed so that extrinsic likelihoods from the ABP algorithm and the decoded estimates from the KV algorithm are fed back to the trellis-based equalizer to form a loop. This significantly improves the code's error correction performance yielding significant coding gains over separate trellis-based equalization and Hermitian decoding. Approaches to improve the performance of the ABP-KV decoder will be introduced. The proposed scheme's iterative behavior will be analyzed by the Extrinsic Information Transfer (ExIT) chart [15] predicting the iterative error correction performance. The interleaved Hermitian codes' performance advantage over interleaved RS codes will also be demonstrated by simulations. It is important to point out that due to the presence of the outer KV algorithm there will be no error floor, unlike LDPC and turbo codes, highlighting the suitability of Hermitian codes for use with data storage channels.

The rest of the paper is organized as follows. Section II presents preliminary knowledge. Section III presents the proposed iterative detection-decoding scheme. Section IV analyzes the iterative scheme utilizing the ExIT chart. Sections V and VI analyze the performance and complexity of the proposal, respectively. Finally, Section VII concludes the paper.

## II. Prerequisite Knowledge

This section presents prerequisite knowledge for the later sections of the paper, including the encoding of interleaved Hermitian codes and the PR channels.

### A. Encoding

Let $\mathbb{F}_q = \{0, 1, \alpha, \cdots, \alpha^{q-2}\}$ denote a finite field of size $q$ where $\alpha$ is a primitive element of the field. Let $\mathbb{F}_q[x, y]$ and $\mathbb{F}_q[x, y, z]$ denote the rings of bivariate and trivariate polynomials defined over $\mathbb{F}_q$, respectively. In this paper, it is assumed that $\mathbb{F}_q$ is an extension field of $\mathbb{F}_2$ such that $q = 2^\zeta$, where $\zeta$ is a positive even integer. The projective Hermitian curve defined in $\mathbb{F}_q$ is:

$$H_w(x, y, z) = x^{w+1} + y^w z + y z^w, \tag{1}$$

where $w = \sqrt{q}$. A one-point Hermitian code is constructed from one of the projective curve's affine components $H_w(x, y, 1) = x^{w+1} + y^w + y$. There are $n = w^3 = q^{\frac{3}{2}}$ affine points that satisfy $H_w(x, y, 1) = 0$, which are of the form $p_j = (x_j, y_j, 1)(1 \le j \le n)$, and a point at infinity $p_\infty = (0, 1, 0)$. A pole basis $\Phi_w$ comprising monomials $\phi_a = \frac{x^\vartheta y^\lambda}{z^{\vartheta+\lambda}}$ is defined on $H_w(x, y, z)$ at $p_\infty$, where $a$ is the index of $\phi_a$ in an ordered list of monomials and $(a, \vartheta, \lambda) \in \mathbb{N}^2$ and $\mathbb{N}$ denotes the set of non-negative integers. In particular, $\vartheta \le w$. With $H_w(x, y, z) = 0$, we have

$$\frac{x}{z} = \frac{y^w + y z^{w-1}}{x^w}, \ \frac{y}{z} = \frac{y^{w+1} + y^2 z^{w-1}}{x^{w+1}}. \tag{2}$$

The order of the monomials $\frac{x}{z}$ and $\frac{y}{z}$ at the point at infinity, $o_{p_\infty}$, becomes obvious with $o_{p_\infty}(\frac{x}{z}) = w$ and $o_{p_\infty}(\frac{y}{z}) = w + 1$. Therefore, the pole order of any monomial in $\Phi_w$ is $o_{p_\infty}(\frac{x^\vartheta y^\lambda}{z^{\vartheta+\lambda}}) = w\vartheta + (w + 1)\lambda$. With $z = 1$ in the affine plane, the monomials $\phi_a$ in the pole basis $\Phi_w$ can be expressed just in terms of $x$ and $y$. They are ordered in terms of increasing pole order and $\Phi_w$ can be defined as [3], [6]

$$\Phi_w = \left\{\phi_a | o_{p_\infty}(\phi_a) < o_{p_\infty}(\phi_{a+1}), \vartheta \le w, a \in \mathbb{N}\right\}, \tag{3}$$

where the $x$-degree $\vartheta$ in all monomials $\phi_a$ is constrained to be less than the $x$-degree of the affine Hermitian curve, $w + 1$, to ensure the generator matrix has independent rows. The generator matrix $\mathbf{G} \in \mathbb{F}_q^{k \times n}$ of an $(n, k)$ Hermitian code is obtained by evaluating the first $k$ monomials in $\Phi_w$ at all $n = q^{\frac{3}{2}}$ affine points following [3]

$$\mathbf{G} = \begin{bmatrix} \phi_0(p_1) & \phi_0(p_2) & \cdots & \phi_0(p_n) \\ \phi_1(p_1) & \phi_1(p_2) & \cdots & \phi_1(p_n) \\ \vdots & \vdots & \ddots & \vdots \\ \phi_{k-1}(p_1) & \phi_{k-1}(p_2) & \cdots & \phi_{k-1}(p_n) \end{bmatrix}, \tag{4}$$

where $n$ is the length and $k$ becomes the dimension of the code. Encoding of a message vector $\overline{F} = [F_1 F_2 \ldots F_k] \in \mathbb{F}_q^k$ is achieved by $\overline{C} = \overline{F} \cdot \mathbf{G} = [C_1 C_2 \ldots C_n] \in \mathbb{F}_q^n$. To perform the ABP decoding, the code's parity-check matrix needs to be known, and it is given as [3]

$$\mathbf{H} = \begin{bmatrix} \phi_0(p_1) & \phi_0(p_2) & \cdots & \phi_0(p_n) \\ \phi_1(p_1) & \phi_1(p_2) & \cdots & \phi_1(p_n) \\ \vdots & \vdots & \ddots & \vdots \\ \phi_{n-k-1}(p_1) & \phi_{n-k-1}(p_2) & \cdots & \phi_{n-k-1}(p_n) \end{bmatrix}. \tag{5}$$

Given that $\xi(x) \in \mathbb{F}_2[x]$ is the minimal polynomial of $\alpha$ over $\mathbb{F}_q$, and $\Xi$ is its companion matrix [16] with size $\zeta \times \zeta$, the binary image of matrix $\mathbf{H}$ can be generated by mapping its entries $\alpha^i \mapsto \Xi^i$, where $i = 0, 1, \ldots, q - 2$. This results in the binary parity-check matrix $\mathbf{H}_b$ of the code with size $(n-k)\zeta \times n\zeta$.

Let $\Lambda$ denote the depth of the block interleaver. After $\Lambda$ independent Hermitian codewords $\overline{C}^{(1)}, \overline{C}^{(2)}, \ldots, \overline{C}^{(\Lambda)}$ have been generated, they will then be interleaved according to the interleaving pattern that writes in symbols vertically and reads the symbols out horizontally, yielding the interleaved Hermitian codewords. They are then converted into binary interleaved coded bit sequences to be written onto the disc. We use $c_t$ to denote the coded bits of a Hermitian codeword and $t = 1, 2, \ldots, n\zeta$, and $c'_t$ to denote the interleaved Hermitian coded bits. Since they are the binary outcome after interleaving $\Lambda$ Hermitian codewords, for $c'_t$, $t = 1, 2, \ldots, \Lambda n\zeta$.

### B. Partial Response Channels

The demand for increasing the storage capacity of magnetic discs requires the packing of more data onto each square inch of the disc. When reading the data, the readback head detects changes in magnetic flux due to changes in the polarity of the write current. The output voltage from the readback head is a positive or negative pulse depending on whether the change in magnetic flux is positive or negative. In longitudinal recording, the transition response is commonly modelled as a Lorentzian pulse [17], whereas in perpendicular recording, the transition

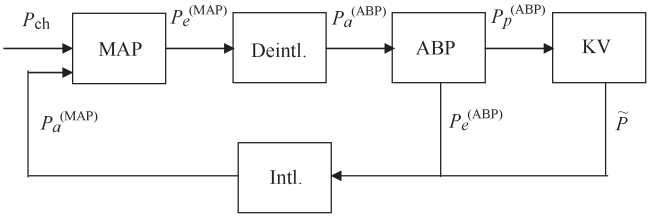


Fig. 1. Structure of the iterative detection-decoding scheme.

response can be modelled using a hyperbolic tangent [18]. For a fixed pulse width, inter-symbol interference (ISI) will increase as the density of recorded bits increases. For magnetic read channels ISI is not eliminated but it is actually shaped by a linear equalizer to have a predetermined response defined by a simple PR polynomial [19] so that ISI is still present after equalization. Given a symbol duration $T$ and channel bandwidth $B$, the maximum transmission rate for binary signalling with no ISI is $\frac{1}{T} = 2B$ [17]. But this cannot be achieved with practical filters. However, if some ISI is still present then the maximum transmission rate of $2B$ symbols/sec. can be achieved.

In this paper, we consider the perpendicular recording channels since it is now the recording method used in modern hard drives. The PR polynomials for perpendicular recording channels are $G(D) = (1+D)^{\varrho}$, where $D$ is a delay unit and $\varrho$ is a positive integer, with a larger value of $\varrho$ indicating more severe ISI. In the rest of the paper, the perpendicular channels that are modelled with the PR polynomials of $G(D) = \frac{1}{\sqrt{6}} + \frac{2}{\sqrt{6}}D + \frac{1}{\sqrt{6}}D^2$ and $G(D) = \frac{1}{\sqrt{20}} + \frac{3}{\sqrt{20}}D + \frac{3}{\sqrt{20}}D^2 + \frac{1}{\sqrt{20}}D^3$ are labelled PR channel I and PR channel II, respectively. The PR polynomials' coefficients ensure there is no channel gain. The linear equalizer is designed to minimize the mean squared error (MSE) between the equalized output and the desired output from the PR polynomial [19]. If the MSE is zero, the magnetic channel and equalizer are equivalent to a channel defined by the PR polynomial. Hence, by making the assumption that the equalized output and desired output are identical then for simulation purposes we can replace the magnetic channel and equalizer with a PR channel to obtain an ideally equalized signal with a controlled amount of ISI. The interleaved coded bits $c'_t \in \{0,1\}$ are mapped to an NRZ signal $x_t \in \{-1,+1\}$. The output of the PR channels $r_t$ is then obtained by first convolving $x_t$ with the impulse response of the PR channel $h_t$ and finally adding additive white Gaussian noise (AWGN) $\eta_t$ with variance $\sigma^2 = \frac{N_0}{2}$ and $N_0$ is the noise power, i.e.,

$$r_t = x_t * h_t + \eta_t. \tag{6}$$

## III. Iterative Detection-Decoding

The iterative detection-decoding scheme is shown in Fig. 1, where the detection and decoding are accomplished by the MAP and the ABP-KV algorithms, respectively. With the channel observations $P_{\text{ch}}$, the MAP detection determines the extrinsic probability $P_e^{(\text{MAP})}$ of the interleaved Hermitian coded bits $c'_t$ and $t = 1, 2, \ldots, \Lambda n\zeta$. They are then deinterleaved and mapped to the *a priori* probabilities $P_a^{(\text{ABP})}$ of the coded bits $c_t$ of each Hermitian codeword and $t = 1, 2, \ldots, n\zeta$. For each Hermitian codeword, the ABP algorithm delivers both the extrinsic probabilities $P_e^{(\text{ABP})}$ and the *a posteriori* probabilities $P_p^{(\text{ABP})}$ for the coded bits. With $P_p^{(\text{ABP})}$, the KV algorithm further decodes the message. If KV decoding yields a message candidate, the deterministic probabilities $\widetilde{P}$ of the Hermitian coded bits will be fed back. Otherwise, the extrinsic probabilities $P_e^{(\text{ABP})}$ will be fed back. They are then interleaved and mapped back to the *a priori* probabilities of the interleaved Hermitian coded bits $P_a^{(\text{MAP})}$ for the next round MAP detection.

### A. MAP Detection

PR equalization is achieved using the MAP algorithm [12]. The trellis-based equalizer is a component of the proposed iterative scheme and takes the *a priori* probabilities $P_a^{(\text{MAP})}(c'_t)$ from either the ABP or KV decoder. Initially, no information is provided by the decoder and the *a priori* probabilities are initialized as $P_a^{(\text{MAP})}(c'_t = 0) = P_a^{(\text{MAP})}(c'_t = 1) = 0.5$. The PR channel has a binary input $c'_t \in \{0,1\}$ and a real output $r_t$. The branch metrics $\gamma_t(s, s')$ of the MAP algorithm corresponding to the state transitions in the trellis diagram are

$$\gamma_t(s,s') = \frac{1}{\sqrt{2\pi\sigma^2}} e^{-\frac{(r_t - x(s,s'))^2}{\sigma^2}} \cdot P_a^{(\text{MAP})}(c'_t), \tag{7}$$

where $x(s, s')$ denotes the trellis output for a transition from an initial state $s$ to the next state $s'$ and $x(s, s') \in \{-1, 1\}$. The MAP equalizer generates the likelihoods $P(c'_t|r_t)$ of the interleaved coded bits $c'_t$ and the extrinsic probabilities $P_e^{(\text{MAP})}(c'_t)$ are obtained from

$$P_e^{(\text{MAP})}(c'_t) = \mathcal{N} \frac{P(c'_t|r_t)}{P_a^{(\text{MAP})}(c'_t)}, \tag{8}$$

where $\mathcal{N} = \sum_{c'_t \in \{0,1\}} P_e^{(\text{MAP})}(c'_t)$ is a normalization factor. They are then deinterleaved and passed to the ABP-KV decoder. Since a codeword symbol can be decomposed into $\zeta$ bits, every $\zeta$ pairs of extrinsic probabilities $(P_e^{(\text{MAP})}(c'_t = 0), P_e^{(\text{MAP})}(c'_t = 1))$ that correspond to a codeword symbol are grouped together during the deinterleaving process.

### B. ABP Decoding

The decoding of a Hermitian code is accomplished by the ABP-KV algorithm [10]. The ABP decoding enhances the bitwise reliability information for KV decoding. Furthermore, it delivers the extrinsic probabilities of the Hermitian coded bits for the iterative detection-decoding.

After deinterleaving, and by reading out each row of the deinterleaver, the following mapping is realized

$$P_e^{(\text{MAP})}(c'_t) \mapsto P_a^{(\text{ABP})}(c_t), \tag{9}$$

and the *a priori* probability for each coded bit $c_t$ of a Hermitian codeword can be obtained, where $t = 1, 2, \ldots, n\zeta$. The *a priori* log-likelihood ratio (LLR) of $c_t$ is determined by

$$L_{a,t} = \ln\left(\frac{P_a^{(\text{ABP})}(c_t = 0)}{P_a^{(\text{ABP})}(c_t = 1)}\right), \tag{10}$$

and the *a priori* LLR vector of a Hermitian codeword is

$$\overline{L}_a = \left[L_{a,1}\, L_{a,2}\, \ldots\, L_{a,(n-k)\zeta}\, \ldots\, L_{a,n\zeta}\right]. \tag{11}$$

The high density of 1 s in $\mathbf{H}_b$ of the Hermitian code must be reduced before belief propagation (BP) decoding starts. This is achieved by the bit reliability oriented Gaussian elimination. Since a higher magnitude of $|L_{a,t}|$ implies the bit is more reliable, the ABP algorithm sorts the *a priori* LLR values according to their magnitudes, yielding an updated bit index sequence $\delta_1, \delta_2, \ldots, \delta_{(n-k)\zeta}, \ldots, \delta_{n\zeta}$. It implies $|L_{a,\delta_1}| < |L_{a,\delta_2}| < \cdots < |L_{a,\delta_{(n-k)\zeta}}| < \cdots < |L_{a,\delta_{n\zeta}}|$ and bits $c_{\delta_1}, c_{\delta_2}, \ldots, c_{\delta_{(n-k)\zeta}}$ are the $(n-k)\zeta$ least reliable bits. Let $\Theta = \{\delta_1, \delta_2, \ldots, \delta_{(n-k)\zeta}\} \subseteq \{1, 2, \ldots, n\zeta\}$ denote the set of unreliable bit indices and $|\Theta| = (n-k)\zeta$. Its complementary set is $\Theta^c = \{\delta_{(n-k)\zeta+1}, \delta_{(n-k)\zeta+2}, \ldots, \delta_{n\zeta}\}$. Based on $\Theta$, the sorted *a priori* LLR vector becomes

$$\overline{L}_a^{\Theta} = \left[L_{a,\delta_1}\, L_{a,\delta_2}\, \cdots\, L_{a,\delta_{(n-k)\zeta}}\, \cdots\, L_{a,\delta_{n\zeta}}\right]. \tag{12}$$

Gaussian elimination will be performed on the matrix $\mathbf{H}_b$, reducing the columns that correspond to the unreliable bits to weight-1 columns. Let $\Upsilon_\delta$ denote the weight-1 column vector with 1 at its $\delta$th entry and 0 elsewhere. For matrix $\mathbf{H}_b$, Gaussian elimination reduces column $\delta_1$ to $\Upsilon_1$, then reduces column $\delta_2$ to $\Upsilon_2$, and etc. Gaussian elimination reduces the first $(n-k)\zeta$ independent columns implied by $\overline{L}_a^{\Theta}$ to weight-1 columns, resulting in an adapted parity-check matrix $\mathbf{H}_b'$ with which the BP decoding is performed. Let $h_{ut} \in \{0, 1\}$ denote the entry of matrix $\mathbf{H}_b'$ and $\mathbf{U}(t) = \{u | h_{ut} = 1,\ \forall\ 1 \le u \le (n-k)\zeta\}$ and $\mathbf{T}(u) = \{t | h_{ut} = 1,\ \forall\ 1 \le t \le n\zeta\}$. The iterative BP process is performed based on the Tanner graph defined by $\mathbf{H}_b'$, yielding the extrinsic LLR value for each Hermitian coded bit by

$$L_{e,t} = \sum_{u \in \mathbf{U}(t)} 2\tanh^{-1}\left(\prod_{\tau \in \mathbf{T}(u)\backslash t} \tanh\left(\frac{L_{a,\tau}}{2}\right)\right). \tag{13}$$

After a number of BP iterations, the *a posteriori* LLR of each Hermitian coded bit can be determined by

$$L_{p,t} = L_{a,t} + \varphi L_{e,t}, \tag{14}$$

where $\varphi \in (0, 1]$ is the damping factor (DF). Therefore, the *a posteriori* LLR vector of a Hermitian codeword is

$$\overline{L}_p = \left[L_{p,1}\, L_{p,2}\, \ldots\, L_{p,(n-k)\zeta}\, \ldots\, L_{p,n\zeta}\right]. \tag{15}$$

To reduce the BP decoding complexity, the Min-Sum algorithm can be utilized with the extrinsic LLRs defined by

$$L_{e,t} = \sum_{u \in \mathbf{U}(t)} \left(\prod_{\tau \in \mathbf{T}(u)\backslash t} \operatorname{sign}(L_{a,\tau}) \cdot \min_{\tau \in \mathbf{T}(u)\backslash t} \{|L_{a,\tau}|\}\right), \tag{16}$$

where for any $\psi \in \mathbb{R}$, $\operatorname{sign}(\psi) = 1$ if $\psi \ge 0$, or $\operatorname{sign}(\psi) = -1$ otherwise. The Min-Sum algorithm is more effective in decoding long Hermitian codes because the matrix $\mathbf{H}_b'$ of these long codes still has a large number of short cycles,[1] which affects the extrinsic LLR calculation in (13).

It can be seen that the ABP algorithm reduces the columns that correspond to the unreliable bits to weight-1 columns. Consequently, it prevents the propagation of the unreliable information during the BP calculation. With the assistance of the reliable information, the LLR values of the unreliable bits are likely to be improved. Note that there can be multiple Gaussian eliminations. If so, the *a posteriori* LLR vector needs to be mapped to the *a priori* LLR vector by $\overline{L}_p \mapsto \overline{L}_a$. The next round of bit reliability sorting and Gaussian elimination will be performed based on the updated $\overline{L}_a$. As a result, the ABP decoding becomes iterative. Each ABP iteration consists of bit reliability sorting, Gaussian elimination and BP decoding which is also iterative. Together with the iterative detection-decoding, there are three types of iterations in the proposed scheme. We call the detection-decoding iteration as the global iteration and use $N_1$, $N_2$, and $N_3$ to denote the designed number of global iteration, ABP iteration and BP iteration, respectively.

The extrinsic and *a posteriori* probabilities of the Hermitian coded bits can be further determined by

$$P_e^{(\mathrm{ABP})}(c_t = 0) = \frac{1}{1 + e^{-L_{e,t}}},\ P_e^{(\mathrm{ABP})}(c_t = 1) = \frac{1}{1 + e^{L_{e,t}}}, \tag{17}$$

$$P_p^{(\mathrm{ABP})}(c_t = 0) = \frac{1}{1 + e^{-L_{p,t}}},\ P_p^{(\mathrm{ABP})}(c_t = 1) = \frac{1}{1 + e^{L_{p,t}}}. \tag{18}$$

### C. KV Decoding

With the *a posteriori* probabilities of (18), a $q \times n$ reliability matrix $\mathbf{\Pi}$ for each Hermitian codeword can be formed. Its entry $\pi_{ij}$ is the symbol wise *a posteriori* probability and

$$\pi_{ij} = P_p(C_j = \rho_i), \tag{19}$$

where $\rho_i \in \mathbb{F}_q$ with $i = 1, 2, \ldots, q$ and $j = 1, 2, \ldots, n$. During the formation, $\zeta$ pairs of *a posteriori* probability values $(P_p^{(\mathrm{ABP})}(c_t = 0), P_p^{(\mathrm{ABP})}(c_t = 1))$ that correspond to a codeword symbol will be multiplied by $q$ different permutations, yielding a column of matrix $\mathbf{\Pi}$. It will then be proportionally transformed into a multiplicity matrix $\mathbf{M}$ of the same size and its entries $m_{ij} \in \mathbb{N}$ [7]. The interpolation process is dependent on the entries of $\mathbf{M}$, yielding a polynomial $Q \in \mathbb{F}_q[x, y, z]$ that interpolates each point $(p_j, \rho_i)$ with a multiplicity of $m_{ij}$ [8]. In general, $Q = \sum_{a,b} Q_{ab} \phi_a z^b$ and its $x$-degree is confined within $w$ by the property of the affine curve, i.e., $x^{w+1} = y^w + y$. Finally, factorization is performed to find the $z$-roots of $Q$, delivering [20], [21]

$$\mathcal{L} = \{f \in \mathbb{F}_q[x, y] \,|\, Q(x, y, f) = 0\}. \tag{20}$$

The coefficients of $f$ form a decoded message vector, which becomes a candidate in the decoding output list $\mathcal{L}$. Let $l = \deg_z Q$

[1] In the adapted matrix $\mathbf{H}_b'$ of the (512, 460) Hermitian code, the amount of short cycles will be around $1.15 \times 10^{10}$.

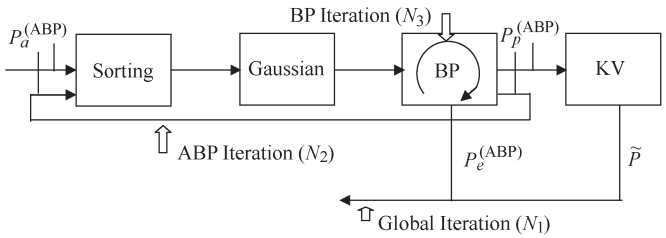


Fig. 2. Functional steps of the ABP-KV decoding.

denote the designed factorization output list size, and $|\mathcal{L}| \leq l$. It determines the error correction capability of KV decoding. Since KV decoding is performed after each ABP iteration, the ABP-KV decoding of a Hermitian codeword will provide at most $lN_2$ message candidates among which the maximum likelihood (ML) criterion will be utilized to select the decoding output. However, notice that in practice, the decoding output list $\mathcal{L}$ often contains only a single candidate. If the KV algorithm provides a decoding output, the deterministic probabilities of the corresponding Hermitian coded bits can be obtained. Let $\hat{c}_t \in \{0,1\}$ denote estimation of the decoded bit, the deterministic probability of bit $c_t$ is determined by

$$\begin{cases} \tilde{P}(c_t=0)=1,\ \tilde{P}(c_t=1)=0, & \text{if } \hat{c}_t=0; \\ \tilde{P}(c_t=0)=0,\ \tilde{P}(c_t=1)=1, & \text{if } \hat{c}_t=1. \end{cases} \tag{21}$$

### D. ABP-KV Decoding Feedback

Summarizing the above mentioned ABP-KV decoding, Fig. 2 shows its functional steps and the probabilities that are being iterated. Moreover, the global, ABP and BP iterations are also indicated with their designed iteration numbers.

After KV decoding of all the $\Lambda$ Hermitian codes, deterministic probabilities $\tilde{P}$ of the decoded bits and extrinsic probabilities $P_e^{(\mathrm{ABP})}$ of the undecoded bits will be given as feedback for the next round of MAP detection. After interleaving, they are mapped back to the *a priori* probabilities $P_a^{(\mathrm{MAP})}$ of the interleaved Hermitian coded bits as

$$P_e^{(\mathrm{ABP})}(c_t), \quad \tilde{P}(c_t) \mapsto P_a^{(\mathrm{MAP})}(c'_t). \tag{22}$$

Note that for $c'_t$, $t = 1, 2, \ldots, \Lambda n\zeta$. Hence, the next round of MAP detection functions with a portion of known *a priori* information, which helps to yield a more accurate detection outcome. At the same time, the extrinsic probabilities of the undecoded bits will be further iterated, allowing them to be decoded in later iterations. The iterative scheme terminates once all $\Lambda$ Hermitian codewords have been decoded, or the designed global iteration number $N_1$ is reached. The decoded Hermitian codeword will not be decoded again in the following iterations. Hence, the next time MAP detection runs, only the extrinsic probabilities of the undecoded bits will be determined by (8). This requires the system to know the identities of the undecoded bits. We can use a binary indicator of size $\Lambda n\zeta$ indicating each coded bit's decoding status. Information of the indicator will also be interleaved alongside the probabilities $P_e^{(\mathrm{ABP})}(c_t)$, $\tilde{P}(c_t)$, so that the MAP detector knows the identity of the undecoded bits.

### E. Performance Improvement Approaches

The performance of the iterative detection-decoding scheme can be further improved by strengthening the ABP-KV decoding and more Hermitian codewords can be decoded within an iteration, feeding back more known *a priori* information for the MAP detection. To improve KV decoding performance, we can increase the designed factorization output list size $l$ [8]. To improve the ABP decoding performance, we can try to restructure the unreliable bit indices group $\Theta$, spinning out a number of independent ABP-KV decodings. E.g., with $\chi < \min\{k\zeta, (n-k)\zeta\}$, we can restructure $\Theta$ as $\Theta = \{\delta_{(n-k)\zeta+1}, \ldots, \delta_{(n-k)\zeta+\chi}, \delta_1, \ldots, \delta_{(n-k)\zeta-\chi}\}$. The sorted *a priori* LLR vector $\overline{L}_a^{\Theta}$ becomes

$$\overline{L}_a^{\Theta} = \big[L_{a,\delta_{(n-k)\zeta+1}} \cdots L_{a,\delta_{(n-k)\zeta-\chi}} L_{a,\delta_{(n-k)\zeta-\chi+1}} \cdots L_{a,\delta_{(n-k)\zeta}} L_{a,\delta_{(n-k)\zeta+\chi+1}} \cdots L_{a,\delta_{n\zeta}}\big]. \tag{23}$$

The following Gaussian elimination will be performed based on the above sorted vector. Such an attempt is proposed based on the observation that the Hermitian coded bits of the original set $\Theta^c$ can also be wrongly estimated by their LLR values. With their corresponding columns being reduced to weight-1, they are granted an opportunity to be corrected by the BP decoding. Details of such an approach can be found in [10].

## IV. ExIT Chart Insights

This section utilizes the ExIT chart to provide insight into the proposed iterative scheme. It sheds lights on the system's error correction performance by predicting the channel signal-to-noise ratio (SNR) threshold over which the interleaved Hermitian coded system's BER starts to fall. We call the SNR threshold the pinch-off SNR limit and denote it as $\mathrm{SNR}_{\mathrm{off}}$.

Let $\mathcal{I}_a^{(\mathrm{DET})}$ and $\mathcal{I}_e^{(\mathrm{DET})}$ denote the mutual information of the *a priori* probabilities and the extrinsic probabilities of the MAP detector, respectively. Similarly, $\mathcal{I}_a^{(\mathrm{DEC})}$ and $\mathcal{I}_e^{(\mathrm{DEC})}$ denote the mutual information of the *a priori* probabilities and the extrinsic probabilities of the ABP-KV decoder. Since the decoder can feedback both the extrinsic and the deterministic probabilities, in calculating $\mathcal{I}_e^{(\mathrm{DEC})}$, the feedback of $\Lambda$ Hermitian decoding outcomes are taken as a common entity without distinguishing the probability feature. That implies

$$\mathcal{I}_e^{(\mathrm{DEC})} = \frac{1}{\Lambda n\zeta} \sum_{t=1}^{\Lambda n\zeta} \mathcal{H}_b\left(P^{(\mathrm{DEC})}(c_t)\right), \tag{24}$$

where $P^{(\mathrm{DEC})}(c_t) = \tilde{P}(c_t)$ if bit $c_t$ is decoded, or $P^{(\mathrm{DEC})}(c_t) = P_e^{(\mathrm{ABP})}(c_t)$ otherwise. $\mathcal{H}_b(P^{(\mathrm{DEC})}(c_t))$ is the binary entropy function that is defined as

$$\mathcal{H}_b\left(P^{(\mathrm{DEC})}(c_t)\right) = -\sum_{c_t \in \{0,1\}} P^{(\mathrm{DEC})}(c_t) \log_2 P^{(\mathrm{DEC})}(c_t). \tag{25}$$

Let $\mathcal{T}^{(\mathrm{DET})}$ and $\mathcal{T}^{(\mathrm{DEC})}$ denote the extrinsic-*a priori* transfer functions of the MAP detector and the ABP-KV decoder, respectively. By realizing the MAP detector as the inner signal

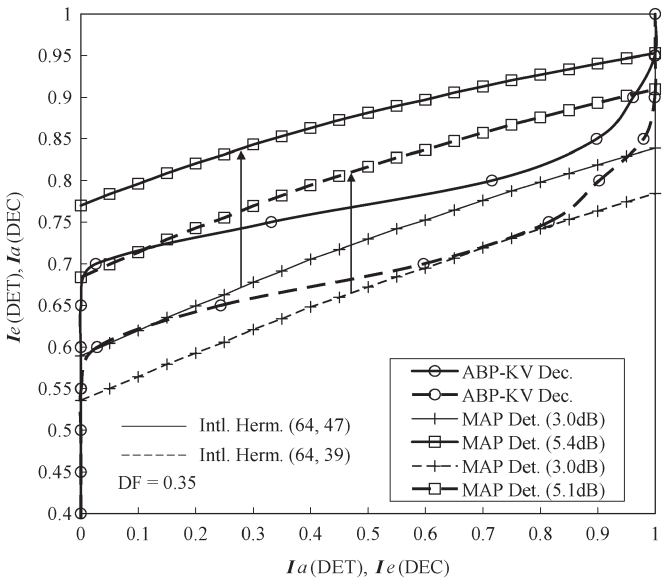


Fig. 3. Exit analysis of iterative detection-decoding of interleaved Hermitian codes over PR channel I.

processing block that takes the channel observations, the ExIT curve of the MAP detector shows

$$\mathcal{I}_e^{(\mathrm{DET})} = \mathcal{T}^{(\mathrm{DET})}\left(\mathcal{I}_a^{(\mathrm{DET})}, \mathrm{SNR}\right). \tag{26}$$

Similarly, the ExIT curve of the ABP-KV decoder shows

$$\mathcal{I}_e^{(\mathrm{DEC})} = \mathcal{T}^{(\mathrm{DEC})}\left(\mathcal{I}_a^{(\mathrm{DEC})}\right). \tag{27}$$

During iterations, mappings of (9) and (22) enable $\mathcal{I}_a^{(\mathrm{DEC})} = \mathcal{I}_e^{(\mathrm{DET})}$ and $\mathcal{I}_a^{(\mathrm{DET})} = \mathcal{I}_e^{(\mathrm{DEC})}$. Hence, by plotting the ExIT curve of the MAP detector and the inverted ExIT curve of the ABP-KV decoder, the interplay between the detector and decoder can be realized. In particular, a tunnel should exist between the two curves such that the iterative system is functioning with a tendency of delivering a zero bit error probability. The SNR value that just yields an exit tunnel between the two curves is the pinch-off SNR limit.

Fig. 3 shows the ExIT chart of the interleaved Hermitian coded systems over PR channel I. The depth of the block interleaver is $\Lambda = 10$. The ABP decoding is functioning with $N_2 = 2$ and $N_3 = 2$, and KV decoding is functioning with $l = 10$. It can be observed that ABP-KV decoding of the interleaved (64, 39) Hermitian code yields a better extrinsic-*a priori* transfer characteristics. This is due to the fact that with the same decoding approach, the low rate code has a better error correction capability. It results in more deterministic probabilities being produced within an iteration. Consequently, the iterative system yields a lower $\mathrm{SNR}_{\mathrm{off}}$ value, i.e., 5.1 dB for the interleaved (64, 39) Hermitian code. While for the interleaved (64, 47) Hermitian code, $\mathrm{SNR}_{\mathrm{off}} = 5.4$ dB. Therefore, the BER curves of iterative detecting-decoding of the two interleaved Hermitian codes are predicted to fall at 5.1 dB and 5.4 dB, respectively. Such a prediction will be validated by simulations in the following section.

TABLE I
INTERLEAVED (64, 39) HERMITIAN CODE OVER PR CHANNEL I AT 7 dB

| $\Lambda$ | 1 | 5 | 10 | 15 |
|---|---|---|---|---|
| BER | $1.31 \times 10^{-3}$ | $3.73 \times 10^{-5}$ | $1.25 \times 10^{-5}$ | $3.78 \times 10^{-5}$ |

TABLE II
INTERLEAVED (64, 47) HERMITIAN CODE OVER PR CHANNEL II AT 8 dB

| $\Lambda$ | 1 | 5 | 10 | 15 |
|---|---|---|---|---|
| BER | $4.76 \times 10^{-3}$ | $8.04 \times 10^{-5}$ | $6.04 \times 10^{-5}$ | $5.07 \times 10^{-5}$ |

## V. PERFORMANCE ANALYSIS

This section analyzes the BER performance of the proposed iterative detection-decoding of interleaved Hermitian codes on the PR channels. Let us recall $N_1$, $N_2$, and $N_3$ are the designed number of global iteration, ABP iteration and BP iteration, respectively, and $l$ is the designed factorization output list size of KV decoding. In the simulation, the ABP decoding is functioning with $N_2 = 2$ and $N_3 = 2$. Unless otherwise stated, KV decoding is functioning with $l = 10$. There are many possibilities for $(N_2, N_3)$, but the above setup yields the best BER performance after a heuristic search. The indicated damping factor is chosen heuristically to optimize the decoding performance. Our comparison benchmarks include Sakata's algorithm and the ABP-KV algorithm, both of which use the MAP detection but without iterative detection-decoding.

The block interleaver depth is $\Lambda = 10$ which is of sufficient size to benefit the iterative signal recovering scheme. This is demonstrated in Tables I and II which show the iterative detection-decoding performance of two interleaved Hermitian codes over the PR channels with $N_1 = 10$. Considering the performance-complexity tradeoff, 10 is an appropriate choice of the interleaver depth on the PR channels. It has been observed that over both of the PR channels, the output of the MAP detector contains many short burst errors of around 6 bits *and* individual bit errors. However, it is still necessary to have a sufficiently large block interleaver to maximize the iterative detection-decoding performance. With a larger block interleaver, more Hermitian decoding events take place within a global iteration and it is likely that more deterministic probabilities can be fed back for the MAP detection. The deterministic probabilities are beneficial for the global iteration as it improves the next round of MAP detection by considering more Hermitian codewords to be decoded later.

An alternative decoding approach for interleaved codes is the collaborative decoding [22], which can almost double the number of burst errors that can be decoded. However, the approach treats a single bit error as it does an burst error, implying it is unsuited for the channels exhibiting both burst and many bit errors. As mentioned, we have observed that the output of MAP detection over both PR channels behave like this.

Figs. 4 and 5 show the performance of the interleaved (64, 39) and (64, 47) Hermitian codes on PR channel I, respectively. They show significant coding gains can be achieved over the benchmark schemes. For the interleaved (64, 47) Hermitian code, the iterative scheme with 2 to 20 global iterations allows the code to achieve 1 dB to 1.8 dB coding gain at the BER of $10^{-5}$ over Sakata's algorithm. It demonstrates the merits of the turbo-like detection-decoding scheme for interleaved

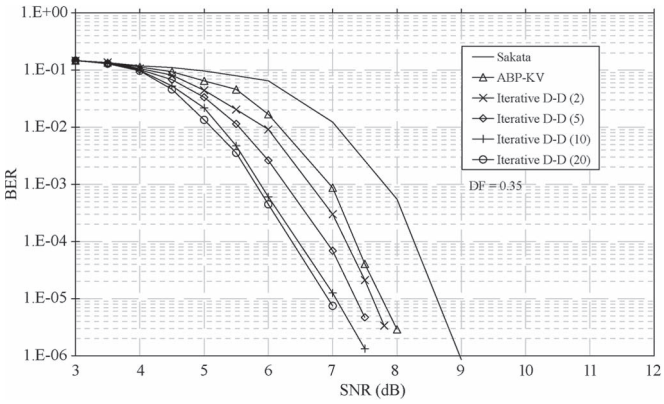


Fig. 4. Performance of the interleaved (64, 39) Hermitian code on PR channel I.

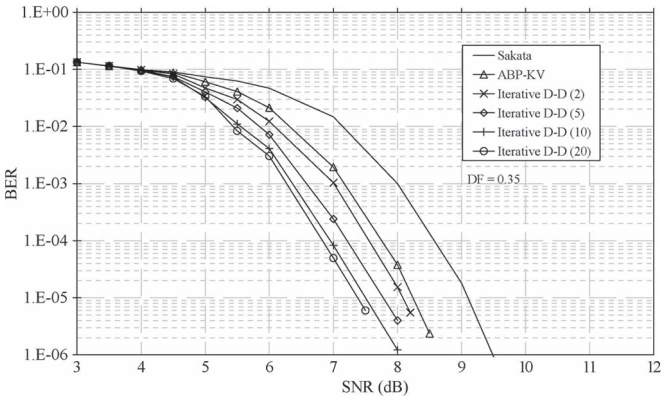


Fig. 5. Performance of the interleaved (64, 47) Hermitian code on PR channel I.

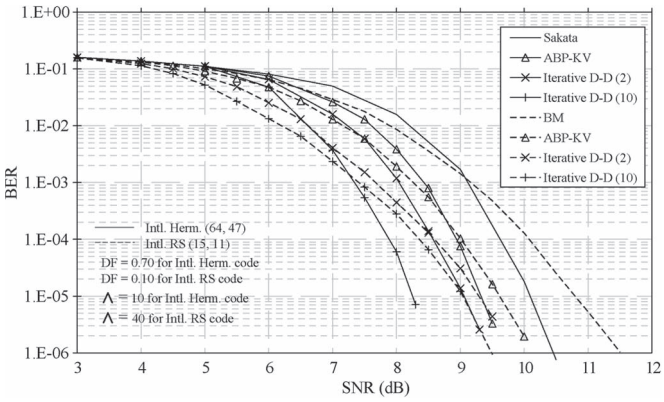


Fig. 6. Performance of the interleaved (64, 47) Hermitian code on PR channel II.

Hermitian codes. The presented results also validate the ExIT chart analysis of Section IV by showing the BER curves start to fall at the predicted $\mathrm{SNR}_{\mathrm{off}}$ values.

Fig. 6 compares the performance of the interleaved (64, 47) Hermitian code with the interleaved (15, 11) RS code on PR channel II which has a more severe level of ISI. Both of the codes are defined in $\mathbb{F}_{16}$ and have a similar code rate. To ensure a fair comparison, the depth of the block interleaver for the interleaved RS code is set to $\Lambda = 40$ so that both of the interleaved codes have a similar length. It can be seen that BER performance of the interleaved Hermitian code achieves a greater error probability decay rate, resulting in a significant performance gain over the interleaved RS code. This is due to

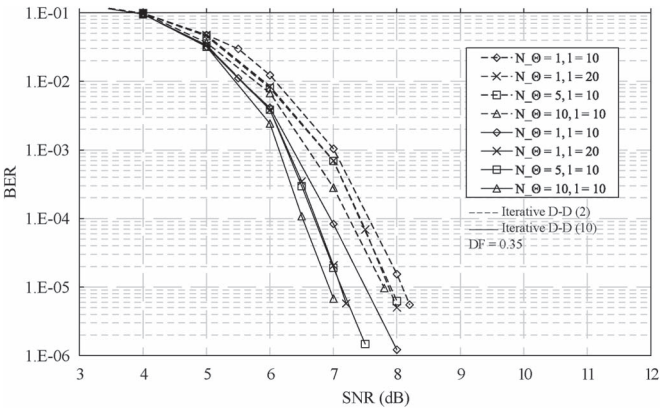


Fig. 7. Improved performance of the interleaved (64, 47) Hermitian code on PR channel I.

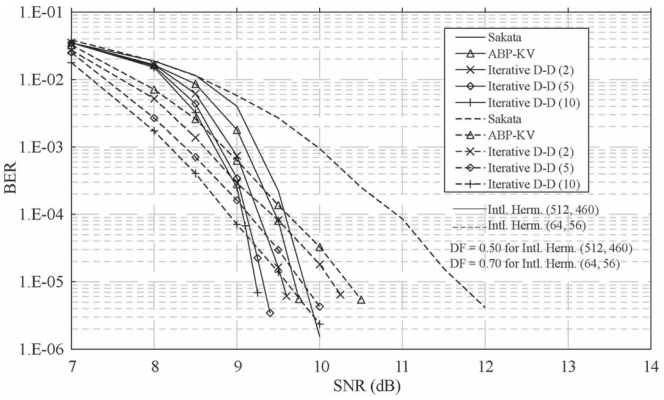


Fig. 8. Performance of the interleaved (512, 460) Hermitian code on PR channel II.

the longer Hermitian code having a larger minimum Hamming distance, and consequently inherits a greater error correction capability. Moreover, by comparing the result of Fig. 5, it can be realized that as the severity of channel ISI increases, the proposed scheme achieves a greater coding gain over the non-iterative benchmark schemes.

To validate the performance improvement approaches mentioned in Section III-E, Fig. 7 shows the performance of the interleaved (64, 47) Hermitian code on PR channel I by strengthening the ABP and KV decodings. Let $N_\Theta$ denote the number of attempts in restructuring the unreliable bit indices group $\Theta$, spinning out $N_\Theta$ independent ABP-KV decodings. It shows that increasing $N_\Theta$ to 5 yields a similar performance as increasing $l$ to 20. However, by increasing $N_\Theta$ to 10, it outperforms the KV decoder-strengthening approach. However, those performance improvement approaches tend to play a less significant role than setting a greater global iteration number $N_1$. Considering they are at the expense of system complexity, moderate ABP-KV decoding parameters are recommended, as exemplified by our simulation setup.

Finally, Fig. 8 shows the performance of the interleaved (512, 460) Hermitian code defined in $\mathbb{F}_{64}$ on PR channel II. To show the advantage of using a long code, its performance is compared with the interleaved (64, 56) Hermitian code with a similar code rate. Due to the large amount of short cycles in matrix $\mathbf{H}'_b$ of the long code, its ABP decoding utilizes the Min-Sum extrinsic

LLR calculation in (16). It shows the long code outperforms the short code with a more significant performance advantage in the deep BER region. Again, this thanks to the long code having a larger minimum Hamming distance. However, notice that iterative decoding of the long code does not achieve as large coding gains over the Sakata and ABP-KV schemes. There are two reasons for this: First, the adapted matrix $\mathbf{H}'_b$ of the long code has a much larger number of short cycles than the short code. Consequently, the ABP algorithm is not as capable in enhancing the soft received information as it for the short code. Second, both codes use a block interleaver of depth 10 and it may not be an ideal size for the long code. However, using a larger interleaver depth for the long code would make the comparison less fair.

## VI. Complexity Analysis

The proposed iterative scheme requires three types of arithmetic computations: floating point, binary and finite field. We now analyze the computational cost of a global iteration. Letting $\Omega^2$ denote the number of trellis states in the MAP detector, the MAP detection requires $O(\Omega\Lambda n\zeta)$ floating point operations. In decoding a Hermitian code, each BP iteration requires $O((n\zeta)^3)$ floating point operations. Hence, the BP decoding dominates the floating point operation. Considering $N_3$ BP iterations will be performed in each of the $N_2$ ABP iterations, a global iteration requires at most $O(N_2N_3\Lambda(n\zeta)^3)$ floating point operations. Each Gaussian elimination requires $O((n\zeta)^3)$ binary operations, and hence a global iteration requires at most $O(N_2\Lambda(n\zeta)^3)$ binary operations. Finally, KV decoding requires $O(n^2l^5)$ finite field operations [8], [23]. Note that [23]'s conclusion on KV decoding complexity for RS codes also holds for Hermitian codes. Considering it is performed for each adapted matrix $\mathbf{H}'_b$, a global iteration requires at most $O(N_2\Lambda n^2l^5)$ finite field operations. In practice, the decoding latency will be dominated by the KV decoding as it requires the more complex finite field operation. However, for long Hermitian codes, e.g., the (512, 460) Hermitian code, the Gaussian elimination and BP decoding will also take a larger portion of the latency as they deal with a large parity-check matrix with a relatively high density.

It is important to point out that the above analysis defines the maximal complexity of a global iteration. Decoding of the interleaved code is performed in a successive cancellation manner meaning that the decoded Hermitian codeword will not be decoded again in any of the following iterations. Therefore, as the global iteration progresses, the number of KV decoding events will be reduced. With a mildly corrupted received information, it is likely that all the codewords are decoded before the final iteration, so the actual computation complexity is channel dependent. The decoding latency can be reduced by parallelizing all the $\Lambda$ outer decoding events. It will be interesting to investigate the consequences of replacing the sophisticated KV decoding with the simpler and less computationally intensive Sakata minimum-distance decoding. Studies have indicated that the performance loss could be relatively minor [10].

[2]In PR channel I $\Omega = 4$, and in PR channel II $\Omega = 8$.

## VII. Conclusion

This paper has proposed an iterative soft detection-decoding scheme for interleaved Hermitian codes that can be employed on magnetic storage channels that exhibit a combination of burst errors and individual bit errors. The proposed scheme integrates the MAP detection and the ABP-KV decoding, enabling the extrinsic probabilities of the Hermitian coded bits to be iterated between the two soft-decision processes. To improve the iterative detection-decoding performance, two ABP-KV decoding performance improvement approaches have been introduced. The ExIT chart analysis of the proposed scheme on the PR channel has been presented, showing the interplay between the soft detector and the soft decoder and highlighting the error correction performance of the proposed scheme. Our performance analysis has shown that significant coding gains can be achieved over conventional schemes that treat the detection and decoding as two separate processes. More importantly, we have also shown the performance advantage of interleaved Hermitian codes over interleaved RS codes, demonstrating the benefit of employing Hermitian codes for high density storage devices. Finally, the computational complexity of the proposed scheme has been analyzed with proposal on more efficient implementation of the iterative scheme.

## References


[1] V. D. Goppa, "Codes on algebraic curves," *Soviet Math*, vol. 24, pp. 75–91, 1981.

[2] M. Johnston and R. A. Carrasco, "Construction and performance of algebraic-geometric codes over awgn and fading channels," *Proc. Inst. Elect. Eng.–Commun.*, vol. 152, no. 5, pp. 713–722, Oct. 2005.

[3] S. Sakata, J. Justesen, Y. Madelung, H. E. Jensen, and T. Hoholdt, "Fast decoding of algebraic-geometric codes up to the designed minimum distance," *IEEE Trans. Inf. Theory*, vol. 41, no. 6, pp. 1672–1677, Nov. 1995.

[4] V. Guruswami and M. Sudan, "Improved decoding of reed-solomon and algebraic-geometric codes," *IEEE Trans. Inf. Theory*, vol. 45, no. 6, pp. 1757–1767, Sep. 1999.

[5] T. Hoholdt and R. R. Nielsen, "Decoding Hermitian codes with sudan's algorithm," in *Proc. Appl. Algebra, Algebraic Algorithms Error-Correcting Codes*, *Lecture Notes in Computer Science*, 1999, pp. 260–270.

[6] L. Chen, R. A. Carrasco, and M. Johnston, "Reduced complexity for list decoding Hermitian codes," *IEEE Trans. Wireless Commun.*, vol. 7, no. 11, pp. 4353–4361, Nov. 2008.

[7] R. Koetter and A. Vardy, "Algebraic soft-decision decoding of reed-solomon codes," *IEEE Trans. Inf. Theory*, vol. 49, no. 11, pp. 2809–2825, Nov. 2003.

[8] L. Chen, R. A. Carrasco, and M. Johnston, "Soft-decision list decoding of Hermitian codes," *IEEE Trans. Commun.*, vol. 57, no. 8, pp. 2169–2176, Aug. 2009.

[9] K. Lee and M. E. O'Sullivan, "Algebraic soft-decision decoding of Hermitian codes," *IEEE Trans. Inf. Theory*, vol. 56, no. 6, pp. 2587–2600, Jun. 2010.

[10] L. Chen, "Iterative soft-decision decoding of Hermitian codes," *IEEE Trans. Commun.*, vol. 61, no. 1, pp. 33–42, Jan. 2013.

[11] M. Fossorier and S. Lin, "Soft-decision decoding of linear block codes based on ordered statistics," *IEEE Trans. Inf. Theory*, vol. 41, no. 5, pp. 1379–1396, Sep. 1995.

[12] L. Bahl, J. Cocke, F. Jelinek, and J. Raviv, "Optimal decoding of linear codes for minimizing symbol error rate," *IEEE Trans. Inf. Theory*, vol. 20, no. 2, pp. 284–287, Mar. 1974.

[13] H. Song, R. M. Todd, and J. R. Cruz, "Low density parity check codes for magnetic recording channels," *IEEE Trans. Magn.*, vol. 36, no. 5, pp. 2183–2186, Sep. 2000.

[14] B. M. Kurkoski, P. H. Siegel, and J. K. Wolf, "Joint message-passing decoding of ldpc codes and partial-response channels," *IEEE Trans. Inf. Theory*, vol. 48, no. 6, pp. 1410–1422, Jun. 2002.

[15] S. ten Brink, "Convergence behavior of iteratively decoded parallel concatenated codes," *IEEE Trans. Commun.*, vol. 49, no. 10, pp. 1727–1737, Oct. 2001.

[16] R. Horn and C. Johnson, *Matrix Analysis*. Cambridge, U.K.: Cambridge Univ., 1985.
[17] J. G. Proakis, *Partial Response Equalization With Application to High Density Magnetic Recording Channels*. Boca Raton, FL, USA: CRC, 2005, ch. 8, pp. 1–23.
[18] M. Madden, M. Oberg, Z. Wu, and R. He, "Read channel for perpendicular magnetic recording," *IEEE Trans. Magn.*, vol. 40, no. 1, pp. 241–246, Jan. 2004.
[19] J. Moon and W. Zeng, "Equalization for maximum likelihood detectors," *IEEE Trans. Magn.*, vol. 31, no. 2, pp. 1083–1088, Mar. 1995.
[20] X. W. Wu and P. Siegel, "Efficient root-finding algortihm with application to list decoding of algebraic-geometric codes," *IEEE Trans. Inf. Theory*, vol. 47, no. 6, pp. 2579–2587, Sep. 2001.
[21] L. Chen, R. A. Carrasco, M. Johnston, and E. G. Chester, "Efficient factorisation algorithm for list decoding algebraic-geometric and reed-solomon codes," in *Proc. IEEE Int. ICC*, May 2007, pp. 851–856.
[22] S. Kampf, "Bounds on collaborative decoding of interleaved Hermitian codes and virtual extension," *Designs, Codes Cryptography*, vol. 70, no. 1/2, pp. 9–25, Jan. 2014.
[23] L. Chen, S. Tang, and X. Ma, "Progressive algebraic soft-decision decoding of reed-solomon codes," *IEEE Trans. Commun.*, vol. 61, no. 2, pp. 433–442, Feb. 2013.

**Li Chen** (S'07–M'08–SM'14) received the B.Sc. degree in applied physics from Jinan University, China, in 2003, and the M.Sc. degree in communications and signal processing and Ph.D. degree in mobile communications in 2004 and 2008, respectively, both from Newcastle University of United Kingdom. From 2010, he joined the School of Information Science and Technology, Sun Yat-sen University of China, where he is now an Associate Professor. He is an Associate Head of the Department of Electronic and Communication Engineering. From 2007 to 2010, he was a Research Associate with Newcastle University. During 2011–12, he is a Visiting Scholar with the Institute of Network Coding, the Chinese University of Hong Kong. He was a recipient of the British Overseas Research Scholarship (ORS). Currently, he is a principle investigator for two National Natural Science Foundation of China (NSFC) projects and a co-investigator of the National Basic Research Program (973 program) project. His primary research interests include: information theory, channel coding and wireless communications.

**Martin Johnston** received the B.Sc. (hons.) degree in physics with electronics from Birmingham University, U.K., in 1999, the M.Sc. degree in electronic engineering from Staffordshire University, U.K., in 2001, and the Ph.D. degree in 2006 from Newcastle University, U.K. From 2006 to 2014 he worked as a Research Associate at the School of Electrical and Electronic Engineering in Newcastle University and he is now working there as a Teaching Fellow. His research interests include the design of advanced error-correcting schemes and low-complexity decoding algorithms for wireless communications and data storage devices.

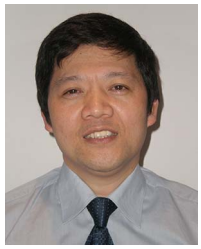

**Gui Yun Tian** (M'01–SM'03) received the B.Sc. degree in metrology and instrumentation and M.Sc. degree in precision engineering from the University of Sichuan, Chengdu, China, in 1985 and 1988, respectively, and the Ph.D. degree from the University of Derby, Derby, U.K., in 1998. From 2000 to 2006, he was a Lecturer, Senior Lecturer, Reader, Professor, and Head of the group of Systems Engineering, respectively, with the University of Huddersfield, U.K. Since 2007, he has been based at Newcastle University, Newcastle upon Tyne, U.K., where he has been Chair Professor in Sensor Technologies. Currently, he is also with School of Automation Engineering, University of Electronic Science and Technology of China. He has coordinated several research projects from the Engineering and Physical Sciences Research Council (EPSRC), Royal Academy of Engineering and FP7, on top of these he also has good collaboration with leading industrial companies such as Airbus, Rolls Royce, BP, nPower and TWI among others.